Journal of Cleaner Production 452 (2024) 142204

Contents lists available at ScienceDirect

Journal of Cleaner Production

journal homepage: www.elsevier.com/locate/jclepro

Investigating the effects of drying on the physical properties of Kombucha Bacterial Cellulose: Kinetic study and modeling approach

Baishali Dey, Sivaraman Jayaraman, Paramasivan Balasubramanian *

Department of Biotechnology & Medical Engineering, National Institute of Technology Rourkela, India, 769 008

ARTICLE INFO

Handling Editor: Prof. Salonitis Konstantinos

Keywords:
Model fitting
Kombucha bacterial cellulose
Hot air oven
Microwave drying
Drying kinetics

ABSTRACT

Kombucha bacterial cellulose (*KBC*), obtained as a by-product of tea fermentation, has potential applications in diverse fields. The high water content and presence of post-fermentation residues necessitate the implementation of suitable drying conditions that can significantly affect the final characteristics of this versatile biopolymer. Thus, to study the effect of different drying methods on its properties, *KBC* was subjected to microwave drying (180–900 W), hot air oven drying (30–70 °C), and shade drying (25 °C). Additionally, the acquired data were fitted into ten different models to study the drying kinetics of *KBC*. The dried sheets were then analyzed to study the changes in water absorption and holding capacity, rehydration, surface color, and other physicomechanical properties (*UTM*, *XRD*, and contact angle analysis). Hence, optimization of the drying conditions will help reduce the time and cost without compromising any of the intrinsic properties that allow it to be processed into various value-added products.

1. Introduction

The increasing awareness of health-promoting benefits associated with probiotic-rich fermented beverages has led to a surge in interest in kombucha, a traditional non- or low-alcoholic fermented tea beverage. Central to the production of kombucha is the symbiotic culture of bacteria and yeast (*SCOBY*), which initiates the fermentation process. This consortium is composed of acetic acid bacteria (*AAB*), lactic acid bacteria (*LAB*), and yeasts (Harrison and Curtin, 2021). A remarkable feature of this consortium is the presence of a cellulose-like pellicle, commonly referred to as "Kombucha bacterial cellulose" (*KBC*), formed on the surface of the fermentation medium as a by-product of the metabolic activity of the specifically chosen strains of *AAB* (Antolak et al., 2021). Cellulose production from kombucha has been reported to be fairly simple, chemically less intensive, and requires a short fermentation duration (Nguyen et al., 2021). This cellulose-rich material holds immense potential for various applications in food packaging (Aduri et al., 2019), biopharmaceuticals (Mousavi et al., 2020), cosmetics (Soares *et al.*, 2021), bioremediation (Gregory et al., 2021), electronics (Kalaiappan *et al.*, 2020), bio-textile (Kamiński *et al.*, 2020), 3D-bioprinting (Pillai *et al.*, 2021) and wound healing (El-Wakil et al., 2019) to name a few. Similar to bacterial cellulose, *KBC* also exhibits high purity, high surface area, hydrophilicity, biodegradability, high crystallinity, biocompatibility, high porosity, non-toxicity, and mechanical strength (Gregory *et al.*, 2021).

Downstream processing of native *KBC* involves harvesting from a fermentation medium, purification, bleaching, and drying. The purpose of the purification of *KBC* is to eliminate the presence of viable cells and liquid culture compounds (metabolites including proteins, peptides, and oligosaccharides) that are adhered to the pellicle. The degree of purification of the cellulose membrane is determined by the thickness of the membrane (Laavanya *et al.*, 2021). On the other hand, in the process of bleaching, hydrogen peroxide or sodium hypochlorite is commonly used for the removal of colored impurities from the cellulose layer (Amarasekara et al., 2020). The final form of purified Bacterial Cellulose (*BC*) can be processed into dried thin films, homogenous fibrous slurry, wet or dry pellicles, etc., depending on its application in industry (Mohamad et al., 2022). For the effective removal of moisture from bacterial cellulose, different drying methods such as oven drying, vacuum oven drying, freeze drying, Buchner funnel oven drying (Bueno et al., 2023), and supercritical drying (Zeng *et al.*, 2014a) have been reported so far. The drying process significantly influences the cellulose pellicle's quality, structure, and mechanical properties (Bodea et al., 2021), directly affecting its potential applications (Ul-Islam *et al.*, 2013). As the moisture content decreases during drying, complex physical and chemical changes occur within the *KBC* structure, impacting its

* Corresponding author.
E-mail address: biobala@nitrkl.ac.in (P. Balasubramanian).

https://doi.org/10.1016/j.jclepro.2024.142204
Received 7 December 2023; Received in revised form 23 February 2024; Accepted 9 April 2024
Available online 11 April 2024

mechanical, thermal, and barrier properties. Efficient preservation and processing of KBC also necessitate understanding it's drying kinetics – a fundamental aspect often overlooked.

In recent years, research in the field of drying kinetics has gained importance, primarily driven by the need to optimize the drying process to retain the primary properties of various products such as fruits (Olanipekun *et al.*, 2015), vegetables (Deng et al., 2018), algae (Agbede *et al.*, 2020), fish (Darvishi *et al.*, 2013), medicinal plants (Bhardwaj *et al.*, 2017) among others. Previous research mainly concentrated on investigating the impact of drying on several aspects of dried bacterial cellulose, including its morphology, crystallinity, water-holding capacity, as well as its mechanical and thermal properties. However, despite the aforementioned studies on the properties and applications of dried *BC*, there is a lack of research and understanding of the impact of drying methods on the kinetic modeling and detailed account of the changes occurring in the physicomechanical properties.

In summary, *KBC* was subjected to different thermo-mechanical drying processes, namely microwave oven (180–900 W), conventional hot air oven (30–70 °C), and shade drying. This work presents a combination of mathematical modeling of the drying kinetics of *KBC* and evaluates the changes occurring in its intrinsic properties to find the optimum parameter under different drying conditions. By characterizing the kinetics of moisture removal, an attempt was made to analyze the impact of drying conditions such as temperature, power levels, and initial moisture content on the final quality of dried *KBC*. The subsequent evaluation of the impact of structural variation on the water absorption capacity (*WAC*), water holding capacity (*WHC*), and rehydration ratio (*RR*) was conducted by subjecting the samples to consecutive cycles of drying and rewetting. The universal testing machine (*UTM*) was utilized to understand the influence of drying conditions on the mechanical properties of *KBC*. Further, the changes occurring in color, crystallinity, and hydrophilicity of *KBC* were investigated using a spectrophotometer, X-ray diffraction method, and drop shape analyzer, respectively, to provide a comprehensive analysis of the changes occurring. The different post-synthetic drying conditions allowed the examination of the relationship between structural variations and the related physicomechanical behavior of differently-dried *KBC* samples.

2. Materials and methods

2.1. KBC cultivation and harvesting

Sweetened tea mixture was prepared by boiling 80 g of sucrose (commercial grade) in 1 L of purified water followed by steeping of 6 g black tea processing waste (procured from *Parry Agro Industries Limited*, Valparai, Tamil Nadu, India) for 5–7 min in a sterilized vessel. After the tea cooled to room temperature, 10% inoculum broth consisting of a symbiotic culture of *Komagataeibacter xylinus* and *Brettanomyces bruxellensis* was added to the sterilized fermentation vessel. The vessel was then covered with a clean and disinfected muslin cloth, secured in place with thread, and kept for static batch fermentation for a period of 10–14 days at room temperature. After the fermentation period, the sweetened tea turned into kombucha, and a cellulose pellicle (*KBC*) was found floating on the surface, which was collected and washed repeatedly with distilled water (*DW*) to remove the tea residues and yeast attached to the bottom surface of the *KBC*. The *DW*-washed pellicles were then soaked in 0.1N sodium hydroxide (NaOH) overnight for further removal of tannins and microbial residues trapped in the *KBC*. After 2–3 overnight soakings of *KBC* with NaOH, it was again washed with *DW* till the pH became neutral. The sheets were cut into 5*5 cm pieces and subjected to different drying conditions followed by diverse characterizations.

2.2. Drying methods of KBC

The cleaned and cut *KBC* samples were weighed using a digital weighing balance (*Shizmadu*) (0.001 accuracy), and thickness was measured using a digital caliper (*Zhart*) (±0.02 mm/0.001" (<100 mm)). The samples were then evenly placed on a glass Petri dish of cross section 100 mm and subjected to different drying conditions.

2.2.1. Microwave drying

The *KBC* sample was subjected to microwave-assisted drying using a household microwave oven (*Electrolux C25K1*51 BG-*CG*) operating at a frequency of 2450 kHz, with power levels varying from 180 to 900 W. The dimensions of the microwave cavity were 190 mm, 310 mm, and 300 mm (height*length*width). The weight during the drying process was recorded at 30-s intervals until a stable weight was achieved.

2.2.2. Hot air oven drying

The convective drying process was conducted using a conventional hot air oven (*BD Instrumentation*) with internal dimensions of 450 mm * 450 mm * 500 mm (length*breadth*depth). The oven was equipped with a temperature sensor positioned at the center and a hot air velocity of 1 m/s with airflow parallel to the Petri dish. The drying temperature varied from 30 to 70 °C. The weight at each moment during the drying process was recorded at 60-s intervals until a stable weight was achieved.

2.2.3. Shade drying

The *KBC* films were carefully positioned within a sterile glass Petri dish and maintained at ambient temperature until the films achieved complete desiccation. The room's temperature was measured to be 25 ± 2 °C, with the relative air humidity fluctuating between 22 and 27 %. The weight at each time interval during the drying process was recorded at 60-s intervals until a stable weight was achieved. The application of shade drying or room temperature (*RT*) drying results in the exertion of capillary pressures by the water meniscus, which in turn applies a compressive force within the pores of the films (**Zeng *et al.*, 2014a**). This compressive force has the potential to induce changes in the density, structure, and porosity of *BC* films.

Following the drying process, the samples were cooled, labeled, and securely packed within zip-lock bags. The storage and transfer of the films for quantification purposes were conducted within a desiccator equipped with a desiccant at the base to prevent any potential inaccuracies in mass loss measurements.

2.3. Data analysis and mathematical modeling

2.3.1. Moisture ratio (MR), drying rate (D_r), and effective diffusivity (D_{eff})

By converting the mass versus time data that was observed into moisture content change with time, the instantaneous moisture content of *KBC* was estimated. Using **Eq. (1)**, the moisture content of the *KBC* (X_t) (dimensionless) after time t in minutes was estimated:

$$X_t = (m_t - m_o) / m_o \quad \text{Eq. (1)}$$

where,

m_t: weight of *KBC* [g] after time (t) [min].

m_o: mass of the wholly dried *KBC* [g].

The moisture content can be transformed into a dimensionless number and expressed as the moisture ratio (*MR*) of *KBC* at different stages of drying, which can be determined by using the following equation Eq. (2):

$$MR = (M_t - M_e) / (M_o - M_e) \quad \text{Eq. (2)}$$

where,

M_t: moisture content at drying time [g/g (dry basis)].

M_o: initial moisture content.

M_e: equilibrium moisture content.

The equilibrium moisture content (M_e) exhibits a relatively smaller value in comparison to M_t or M_o. Therefore, Eq. (2) can be expressed in a

simplified form as Eq. (3) (Perea-Flores et al., 2012)

$$MR = M_t / M_o \quad \text{Eq. (3)}$$

From the moisture content of *KBC*, it is possible to determine the drying rate of *KBC* using the following equation,

$$D_r = (X_{t+\Delta t} - X_t) / \Delta t \quad \text{Eq. (4)}$$

where,

$X_{t+\Delta t}$: moisture content of *KBC* after time $(t + \Delta t)$ [min].

Δt: increment in time [min].

Following Fick's law of diffusion, moisture is gradually lost from the interior cellulose surface to the exterior throughout the thin layer drying process. The distance covered by the migration of water is equal to the thickness of *KBC*. As a result, for ease of calculation, it was assumed that *KBC* was a homogeneous infinite slab, and the slab's thickness was viewed as the distance at which moisture can move during the drying process. **Eq. (5)** can be used to express the relationship between *MR* and D_{eff} (**Wang et al., 2015**),

$$MR = \frac{8}{\pi^2}\sum_{n=1}^{\infty}\frac{1}{n^2} exp\left(-\frac{\pi^2 D_{eff}}{H^2} t\right) \quad \text{Eq. (5)}$$

which can be simplified into **Eq. (6)** for longer drying times,

$$MR = \frac{8}{\pi^2} exp\left(-\frac{\pi^2 D_{eff}}{H^2} t\right) \quad \text{Eq. (6)}$$

where,

D_{eff}: effective moisture diffusivity [$m^2\ s^{-1}$].

H: thickness [m].

t: drying time [s].

For long drying time, the aforementioned expression could be represented linearly as **Eq. (7)**,

$$\ln(MR) = ln\left(\frac{8}{\pi^2}\right) - \left[\frac{D_{eff}\pi^2}{H^2} t\right] \quad \text{Eq. (7)}$$

Thus, the value of effective diffusivity (D_{eff}) [$m^2\ s^{-1}$] value is given by the slope of the straight line produced from the equation by plotting ln*(MR)* vs *t* [min] given by

$$Slope = (\pi^2 D_{eff}) / 4L^2 \quad \text{Eq. (8)}$$

where,

L: thickness of cellulose before drying [m].

2.3.2. Activation energy (E_a)

The relationship between the effective diffusivity (D_{eff}) [$m^2\ s^{-1}$], which is dependent on temperature, and the Arrhenius factor (D_o) [$m^2\ s^{-1}$] as a function of the activation energy (E_a) [kJ mol^{-1}] and the temperature (T) [K] can be provided by the following equation **(Eq. (9))** **(Doymaz and Smail, 2011);**

$$D_{eff} = D_o\ exp\left(-\frac{E_a}{RT}\right) \quad \text{Eq. (9)}$$

where,

R: universal gas constant [8.314 J $mol^{-1}\ K^{-1}$].

By taking logarithm on both sides. **Eq. (9)** can be converted into linear form **Eq. (10)**. The activation energy (E_a) [kJ mol^{-1}] can be calculated by taking the slope of the straight line plotted between ln (D_{eff}) and 1/T,

$$ln(D_{eff}) = ln(D_o) - \frac{E_a}{RT} \quad \text{Eq. (10)}$$

Similar to the oven drying experiments, the activation energy (E_a) [W g^{-1}] of the microwave drying process can be investigated using a modified Arrhenius reaction **(Olanipekun *et al.*, 2015)** **(Eq. (11))**,

$$D_{eff} = D_o exp\left[\frac{E_a m}{P}\right] \quad \text{Eq. (11)}$$

where,

D_o: Arrhenius factor [$m^2\ s^{-1}$].

P: microwave power [W].

m: weight of *KBC* [g].

Calculating the slope of the straight line plotted between ln (D_{eff}) and m/P **(Eq. (12))** will yield the activation energy (E_a) [W g^{-1}]

$$ln(D_{eff}) = ln(D_o) - \frac{E_a m}{P} \quad \text{Eq. (12)}$$

2.3.3. Curve fitting and modeling

The data from the drying methods, using a microwave oven with a power range of 180–900 W, a conventional hot air oven at various temperatures (30–70 °C), and at room temperature, were fitted into different models, as shown in Table 1. The main role in evaluating the goodness of fit lies with the correlation coefficient, showcasing the extent to which an independent variable in a regression model can explain the variance of a dependent variable. A reduced mean square deviation (χ^2) is employed to evaluate the adequacy of data distribution, verify the independence, and estimate confidence intervals around variance. The sum of squared errors (*SSE*) denotes the overall discrepancy between the observed response values and the fit of the model. Root mean square error (*RMSE*) serves as a standard metric for assessing prediction accuracy, depicting the Euclidean distance between actual and expected values. The model exhibiting the most favorable goodness of fit displayed the highest R^2 and the lowest values for χ^2, *SSE*, and *RMSE* **(Biswas *et al.*, 2022)**.

For each of the models employed in the three separate drying setups, the coefficient of determination (R^2), the sum of square error (*SSE*), the root mean square error (*RMSE*), and χ^2 were used to assess the goodness of fit.

$$R^2 = 1 - \frac{\sum_{i-1}^{n}\left(MR_{(exp,i)} - MR_{(pred,i)}\right)^2}{\sum_{i-1}^{n}\left(MR_{(exp,i)} - \overline{MR}\right)^2} \quad \text{Eq. (13)}$$

$$SSE = \frac{1}{N}\sum_{i=1}^{N}\left(M_{RExp,i} - M_{RPred,i}\right)^2 \quad \text{Eq. (14)}$$

Table 1
Different models and their equations for fitting thin layer drying data of *KBC*.

Sl. No.	Model Name	Model Equation	References
1.	Midilli-Kucuk	$M_R = aexp(-kt^n) + bt$	Midilli et al. *(2002)*
2.	Newton	$M_R = exp(-kt)$	Kaya et al. (2007)
3.	Page	$M_R = exp(-kt^n)$	Singh et al. *(2008)*
4.	Logarithmic	$M_R = aexp(-kt) + c$	Wang et al. (2007)
5.	Two-term	$M_R = aexp(-k_0 t) + bexp(-k_1 t)$	Chayjan et al. (2011)
6.	Modified Henderson and Pabis	$M_R = aexp(-kt) + b\exp(-gt) + cexp(-ht)$	Toğrul and Pehlivan (2004)
7.	Wang and Singh	$M_R = 1 + at + bt^2$	Mohapatra and Rao (2005)
8.	Singh	$M_R = \exp(-kt) - akt$	Inyang et al. (2018)
9.	Parabolic model	$M_R = a + bt + ct^2$	Sharma and Prasad (2004)
10.	Vega-Lemus	$M_R = (a + kt)^2$	Guiné (2010)

$$RMSE = \left[\frac{1}{N}\sum_{i=1}^{N}\left(M_{RPred,i} - M_{RExp,i}\right)^2\right]^{1/2} \quad \text{Eq. (15)}$$

$$\chi^2 = \frac{\sum_{i=1}^{N}\left(M_{RExp,i} - M_{RPred,i}\right)^2}{N - z} \quad \text{Eq. (16)}$$

where,

$M_{RExp,\,i}$: experimental values of moisture ratio.
$M_{RPred,\,i}$: predicted values of moisture ratio.
N: number of observations.
z: number of constants.

2.4. Effect of drying on the physicomechanical properties of KBC

2.4.1. Water absorption capacity (WAC)

The dried membranes were submerged in de-ionized (*DI*) water at room temperature until equilibration in order to calculate the *WAC*. The membranes were then taken out of the water, and the extra moisture on their surface was blotted out with tissue paper. The enlarged membrane weights were determined, and the process was repeated until no weight change was seen. The following equations (**Eq. (17)** and (**Eq. (18)**) were used to determine the *WAC* (**Lin *et al.*, 2013**) and moisture content (*MC*) (**Bodea *et al.*, 2021a**), respectively:

$$WAC(\%) = \{(W_h - W_d)/W_d\} \times 100 \quad \text{Eq. (17)}$$

$$MC\ (\%) = \{(W_h - W_d)/W_h\} \times 100 \quad \text{Eq. (18)}$$

where,

W_h: weight of the hydrated membrane [g].
W_d: weight of dry membrane [g].

2.4.2. Water holding capacity (WHC) and rehydration ratio

For measuring the *WHC*, the membranes were submerged in distilled water for an adequate duration until equilibrium was reached. They were then retrieved using tweezers, carefully dried on tissue paper to eliminate any excess surface water, and subsequently weighed (W_{wet}). Then, the completely swollen films underwent a freeze-drying process, and their weight (W_{dry}) was again measured. The calculation of the *WHC* of the samples was done using Eq. (19) (**Stumpf *et al.*, 2013**):

$$WHC = \left(W_{wet} - W_{dry}\right)/W_{dry} \quad \text{Eq. (19)}$$

To measure the rehydration ratio (*RR*), the freeze-dried samples were immersed in distilled water (w/v = 1:2) until swelling weight (W_{reh}) remained constant. Eq. (20) (**Chang and Chen, 2016**) was used to determine the membrane rehydration rate:

$$RR = \{(W_{reh} - W_{dry})/(W_{wet} - W_{dry})\} \times 100 \quad \text{Eq. (20)}$$

2.4.3. Surface color measurement

The surface color of *KBC* was assessed during drying using a spectrophotometer (*Benchtop Spectrophotometer Make: X-rite Model: Ci7600*). A white ceramic plate served as the calibration tool for the apparatus. The *CIE* (*Commission Internationale de l'Éclairage*) color values (*L*, a*, and b**) were measured in order to evaluate the color change of the samples. Where L* stands for the samples' lightness/darkness, *a** for their greenness/redness, and *b** for their blueness/yellowness. Eqs. (21)–(23) was used to calculate the total color difference (ΔE^*), total hue difference (ΔH^*), and total saturation difference (ΔC^*) (**Biswas et al., 2022**):

$$\Delta E^* = \sqrt{(\Delta L^*)^2 + (\Delta a^*)^2 + (\Delta b^*)^2} \quad \text{Eq. (21)}$$

$$\Delta H^* = \sqrt{(\Delta E^*)^2 - (\Delta L^*)^2 + (\Delta C^*)^2} \quad \text{Eq. (22)}$$

$$\Delta C^* = \sqrt{(a^*)^2_{samp} + (b^*)^2_{samp}} - \sqrt{(a^*)^2_{ref} + (b^*)^2_{ref}} \quad \text{Eq. (23)}$$

$\Delta L^* = L^*_{ref} - L^*_{samp}$, $\Delta a^* = a^*_{ref} - a^*_{samp}$, $\Delta b^* = b^*_{ref} - b^*_{samp}$

Ref: Undried *KBC*.
Samp: Dried *KBC*.

2.4.4. Other physical properties

2.4.4.1. UTM analysis. The tensile property of the dried *KBC* membrane was assessed utilizing an *Electroplus E1000 & E3000 test system*. A membrane specimen measuring 1 × 3 cm^2 was affixed to the testing module. The tensile strength and break elongation of the test were evaluated.

2.4.4.2. XRD analysis. The crystallinity of the dried samples was determined using X-ray diffraction (XRD) measurement (*Empyrean: Multi-functional X-Ray Diffraction System, Malvern Panalytical)*. The instrument was operated at 40 kV (kV) and 40 mA (mA) with a Cu source, Ni filter, and *PIXEL1D* detector. The samples underwent scanning in 2θ ranges spanning from 5° to 40°, with a scanning rate of 10° per minute and step size of 0.05. The determination of crystallinity involved integrating the XRD peaks while considering a baseline for each peak (representing the crystalline portion). The total area under the diffractogram was also calculated, using Eq. (24) with a straight line from 5 to 40° 2θ as the baseline (**Ruan *et al.*, 2016**):

$$Crystallinity(\%) = \left\{\sum A_{cryl} \Big/ \left(\sum A_{cryl} + \sum A_{amph}\right)\right\} \times 100 \quad \text{Eq. (24)}$$

where,

ΣA_{cryl}: integrated area of all crystalline peaks.
ΣA_{amph}: integrated area of all amorphous peaks.

Further, d-spacing was calculated using the Bragg's equation (Eq. (25)) (**Zeng et al., 2014**):

$$n\lambda = 2d \sin\theta \quad \text{Eq. (25)}$$

which gives the value of interplanar spacing as in Eq. (26),

$$d = \frac{n\lambda}{2 \sin\theta} \quad \text{Eq. (26)}$$

where,

λ = 1.546 Å (wavelength of incident X-ray).
θ = peak position [radians].
n = 1 (order of diffraction).
d = interplanar spacing [Å].

2.4.4.3. Contact angle measurement. The wettability of the *KBC* film after drying was assessed using a Drop Shape Analyzer (*DSA25, Krüss, Germany*). The sessile drop method was employed to measure the static contact angle of the film, using 3 μL distilled water at ambient temperature. This measurement was conducted in order to determine the hydrophilic or hydrophobic nature of the film. In order for a sample to exhibit wetting properties, it is necessary for the contact angle to fall within the range of 0–90°. Conversely, a hydrophobic sample is characterized by a contact angle exceeding 90°.

The experiments were performed in triplicates and used to compute the means and standard deviations.

3. Results and discussion

3.1. Drying characteristics

3.1.1. Microwave drying characteristics

Fig. 1a illustrates the relationship between the moisture ratio and

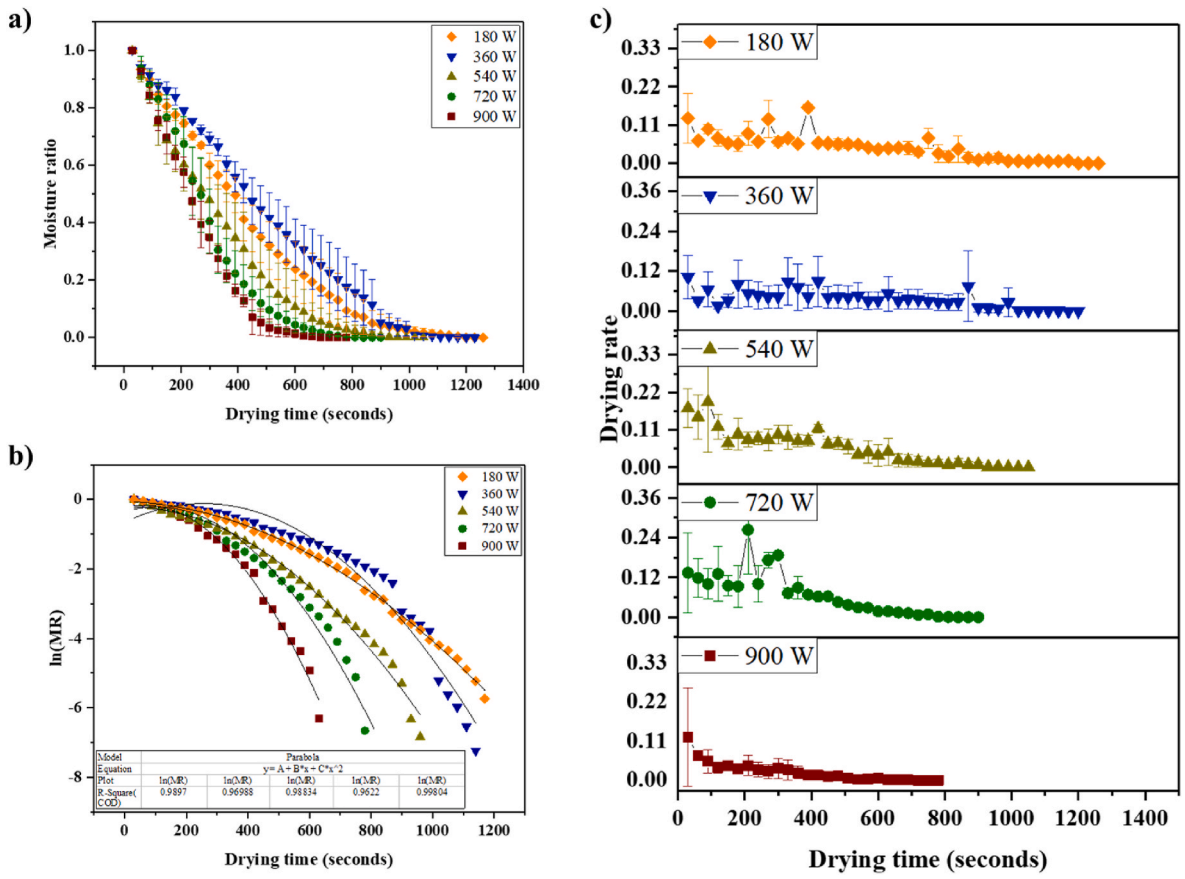

Fig. 1. a) Effect of drying time on the moisture content of *KBC*; b) Plot of ln *MR* vs. drying time; c) Drying rate curves of *KBC* at different power levels in a microwave oven.

drying time during the microwave drying process of *KBC* at different powers (180, 360, 540, 720, and 900 W). The moisture ratio exhibited a decline over the course of the drying process due to the effective evaporation of water molecules from the cellulose pellicle. The rate at which moisture is extracted from the cellulose layer exhibited a positive correlation with the microwave power level. Consequently, the drying duration for *KBC* films decreased as the microwave power level increased. A total moisture content of 98.01 ± 1.14% was effectively removed from the *KBC* sample at different time intervals, specifically at 21, 20, 17, 15, and 13 min, corresponding to the application of microwave powers of 180, 360, 540, 720, and 900 W, respectively, during the drying process. At higher microwave power levels, due to greater production of microwave energy, the generation of heat also gets elevated. This, in turn, speeds up the evaporation of moisture from the cellulose material. Similar trends were also observed and reported by **Behera and Balasubramanian (2021)** and **Agbede et al. (2020)** during the thin layer drying process of microalgal samples.

The effective moisture diffusivity was determined by plotting the data of ln*(MR)* against the drying time for power outputs ranging from 180 to 900 W, as depicted in Fig. 1b, which shows a non-linear relationship between moisture ratio and drying time. The D_{eff} values were calculated from the slope of each line in Fig. 1b using **Eq. (8)**, and the corresponding results are presented in Table 2. The data indicates that the effective moisture diffusivities range from $23.55*10^{-11}$ to $48.27*10^{-11}$ m^2s^{-1} at power levels of 180–900 W, respectively. The increase in moisture diffusivity in direct proportion to the increase in drying microwave power can potentially be attributed to the increased thermal energy. This results in amplified water molecule activity and subsequently leads to an increased moisture diffusivity in samples (**Darvishi *et al.*, 2013**). Similar observations were also reported by

Table 2
Values of effective diffusivity (D_{eff}), Activation energy (E_a), along with total drying time and moisture content removed, for different drying conditions.

Drying conditions	Total drying time (min)	Total removed moisture content (%)	D_{eff} (10^{-11} m^2s^{-1})	E_a (W g^{-1})
Microwave drying				
P_180	21.0	98.64 ± 0.00	23.55	131.70
P_360	20.5	98.66 ± 0.08	29.21	
P_540	17.5	98.54 ± 0.15	30.31	
P_720	15.0	98.39 ± 0.54	40.79	
P_900	**13.0**	98.11 ± 0.38	**48.27**	
Hot air oven drying				
HO_30 °C	38.0	97.89 ± 0.04	10.55	2567.35
HO_50 °C	25.0	98.61 ± 0.03	18.26	
HO-70 °C	**19.0**	98.33 ± 0.14	**28.28**	
Room temperature drying				
RT	61.0	98.06 ± 0.09	6.23	–

(RT: Room temperature, HO: Temperature of hot air oven, P: Microwave power levels).

Aydogdu et al. (2015) and İlter et al. (2018) for eggplant and garlic puree, respectively. Based on **Eq. (11)**, the activation energy (E_a) was calculated by determining the slope of the graph of D_{eff} plotted against m/P and was observed to be 131.70 Wg^{-1}.

During the initial stage of the drying process (Fig. 1c), the *KBC* sample exhibited a significantly elevated moisture content. As a consequence, there was an increased absorption of microwave power and higher rates of drying, which attributed to the enhanced moisture diffusion. As the process of drying advanced, the reduction in moisture content within the cellulose layers led to a decline in the capacity of the product to absorb microwave energy, consequently leading to a decrease

in the rate at which the drying process occurred. At lower moisture levels, it was not possible to distinguish any variations in drying rates among the five microwave power levels. The primary cause of this phenomenon is likely the absence of water following the elimination of unbound moisture, resulting in the redirection of thermal energy towards bond dissociation rather than the heating of water molecules (Nguyen et al., 2019). The experimental results indicated that an increase in microwave output power led to higher rates of drying. Hence, the power level of the microwave had a significant impact on the rate of drying. These findings suggest that the rate of mass transfer is accelerated during high-power microwave heating due to the increased generation of heat within the sample (Demiray et al., 2017). This results in increased variability in vapor pressure between the cellulose layers' center and surface, attributable to the specific volumetric heating effect of microwaves (Zarein *et al.*, 2015), which has the potential to greatly enhance the rate of moisture diffusion, thereby leading to an accelerated drying rate and a corresponding reduction in drying time. The phenomenon referred to as the "pumping effect" denotes a distinctive mass transfer process (Song *et al.*, 2016).

3.1.2. Conventional hot air oven drying characteristics

The variation in moisture content with drying time at 30, 50, and 70 °C has been shown in Fig. 2a. As expected, the time required for the moisture content of *KBC* to reach equilibrium after removal of approximately 98.29 ± 0.39 % was observed to decrease as the drying temperature increased. The plot clearly depicts that the drying of *KBC* is affected by air temperature as the duration required for *KBC* to dry decreased from 38 to 19 min when the drying temperature was elevated from 30 to 70 °C.

The effective moisture diffusivity (D_{eff}) values for *KBC* under various drying temperatures are presented in Table 2 by plotting ln*(MR)* against time (Fig. 2b). The D_{eff} values at temperatures of 30 °C, 50 °C, and 70 °C were measured to be $10.55*10^{-11}$, $18.26*10^{-11}$ and $28.28*10^{-11}$ m^2s^{-1} respectively. The coefficient of moisture diffusion (D_{eff}) exhibits a positive correlation with temperature, as the kinetic energy of water molecules increases with higher temperatures. This heightened molecular movement results in an elevated moisture diffusivity. The values of D_{eff} for *KBC* might be lower compared to other products such as microalgae (Behera and Balasubramanian, 2021), olive waste cake (Vega-Gálvez et al., 2010), onion slices (Demiray *et al.*, 2017), fish (Darvishi *et al.*, 2013) and pineapple slices (Biswas *et al.*, 2022). This may be due to the fact that the phenomenon depends on the drying conditions and the physical-chemical characteristics of the dried products, including factors such as composition and thickness. The activation energy for *KBC* using conventional hot air oven drying was found to be 2567.35 Wg^{-1}. The current findings indicate that the activation energy required for drying of *KBC* in hot air oven is comparatively high. Consequently, the extraction of moisture from *KBC* may pose challenges, indicating that achieving thorough desiccation of the cellulose material would require either an extended drying period or elevated drying temperatures while using a hot air oven.

The change in drying rate with drying time is shown in Fig. 2c. With an increase in drying air temperature, the drying rate increased, and the drying time was lowered. Higher temperatures between the drying air and cellulose layer increase the heat transfer coefficient and also enhance the vapor pressure of water, affecting heat and mass transfer rates. Similar results were also reported by Olanipekun et al. (2015) and Deng et al. (2018) during the drying of pineapple and red pepper. Compared to microwave oven drying, hot air oven drying showed lower drying rates and higher drying time except for 70 °C, which showed comparable drying time and drying rate to that of microwave oven drying at 180 W.

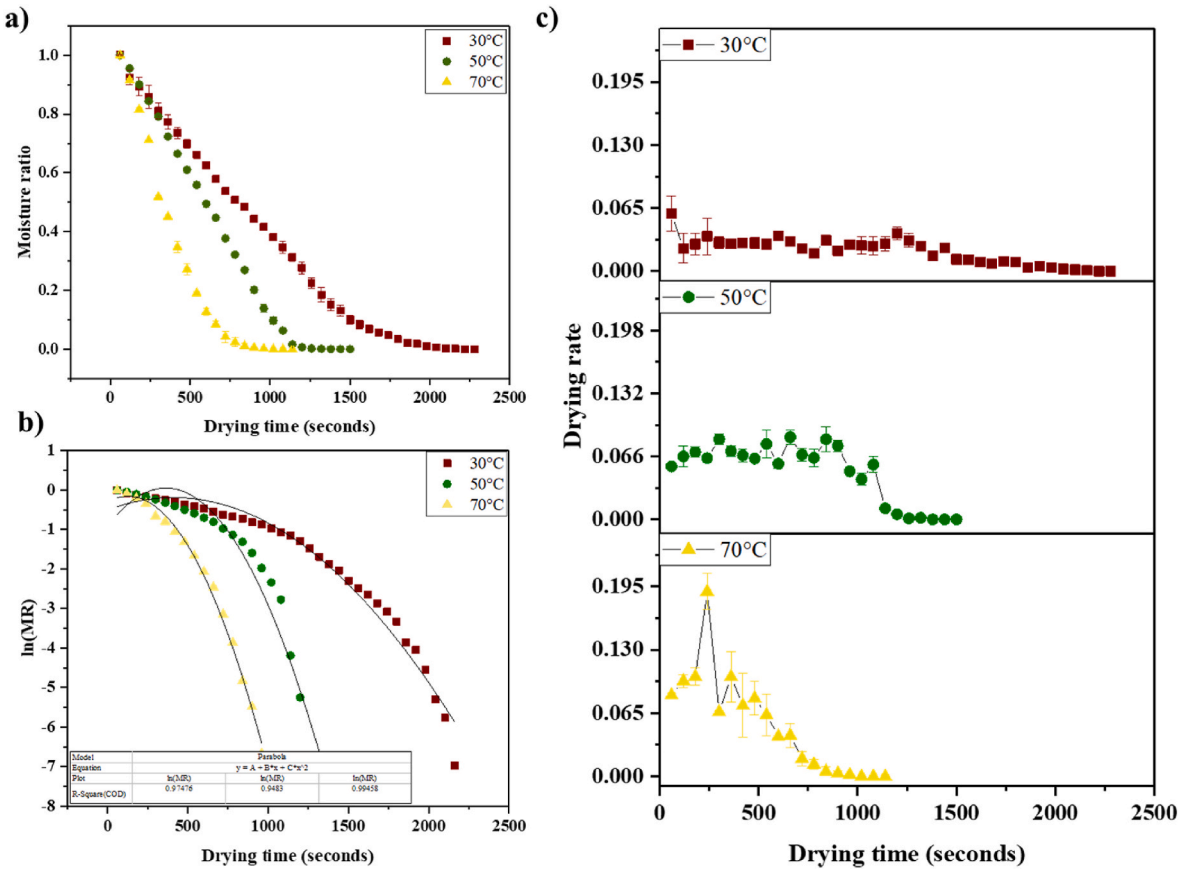

Fig. 2. a) Effect of drying time on the moisture content of *KBC*; b) Plot of ln *MR* vs. drying time; c) Drying rate curves of *KBC* at different temperatures in a hot air oven.

3.1.3. Room temperature drying characteristics

The decrease in moisture ratio with time has been represented in the plot of Fig. 3a. Compared to microwave and hot air oven drying, shade drying or drying at room temperature took the longest time of 61 min to remove total moisture of 98.06 ± 0.09 % from *KBC* (Table 2). Fig. 3b represents the plot between ln*(MR)* against time and the moisture diffusivity was calculated to be $6.23*10^{-11}$ m^2s^{-1}, lower than that of microwave and hot air oven drying. Fig. 3c shows the drying rate of *KBC* at room temperature, which can be seen to be significantly lower than that of microwave and hot air oven drying. The process of drying at room temperature was found to be the most time-consuming as the dehydration processes conducted in shaded environments prevented the exposure of the product to elevated temperatures. The ambient temperature, which had an average value of 25.04 °C, was significantly lower than the optimal temperature of 40 °C. Consequently, this resulted in a deceleration of the dehydration process, also observed by **Alara et al. (2018)**, **Bhardwaj et al. (2017)**, and **Bhardwaj et al. (2019)** during the drying of different medicinal plants.

3.2. Modeling of drying characteristics

3.2.1. Drying kinetics of KBC in microwave

The model with the highest R^2 values and the lowest χ^2 and *RMSE* values was chosen as the one that most accurately described the thin-layer drying characteristics of *KBC* films with microwave drying. The Page model, out of all the examined models, has the highest R^2 (0.9983, 0.9958, 0.9958, 0.9980, 0.9971) value and the lowest values for χ^2 (1.77E-4, 4.70E-4, 3.93E-4, 2.25E-4, 3.24E-4) and *RMSE* (0.0133, 0.0217, 0.0198, 0.0150, 0.0180) for 180 W, 360 W, 540 W, 720 W and 900 W respectively (Table 3). Page is a semi-theoretical model based on Newton's Law of cooling, which is applied to mass transfer. While using this law, it is assumed that conditions are isothermal and that the product's surface is the only area resistant to moisture transfer. They are simplified solutions of Fick's second law **(Inyang et al., 2018)**. **İlter et al. (2018)** and **Demiray et al. (2017)** also reported the page model as the most suitable for explaining the microwave drying of garlic puree and onion slices (*Allium cepa* L.). For the thin layer drying of KBC using the microwave, Page was selected as the most adequate model.

3.2.2. Drying kinetics of KBC in conventional hot air oven

Table 4 represents a range of R^2 values - 0.9275 to 0.9952 (at 30 °C), 0.8763 to 0.9941 (at 50 °C), 0.8925 to 0.9973 (at 70 °C), χ^2 values - 7.39E-3 to 5.12E-4 (at 30 °C), 1.45E-2 to 7.63E-4 (at 50 °C), 1.31E-2E-3 to 3.46E-4 (at 70 °C), *RMSE* values - 0.0226 to 0.0859 (at 30 °C), 0.0276 to 0.1204 (at 50 °C), 0.0186 to 0.1193 (at 70 °C) respectively for conventional hot air oven drying of *KBC* films. For conventional hot air oven drying, the parabolic model showed the highest R^2 (0.9952 (30 °C), 0.9941 (50 °C)) and lowest χ^2 (5.12E-4 (30 °C), 7.63E-4 (50 °C)), *RMSE* (0.0226 (30 °C), 0.0276 (50 °C)) values at lower temperatures but at 70 °C, page model showed highest R^2 (0.9973) and lowest χ^2 (3.46E-4), *RMSE* (0.0186) values. **Singh et al. (2008)** reported the Page model as the best-fit model for the drying of water chestnuts over a range of air temperatures (50–90 °C). It was further reported that the Page model has proven effective in describing the drying behavior of different biological materials. During the drying of pre-treated black grapes at 60 °C, the page model was found to be the most suitable in describing its drying curves (**Doymaz, 2006**). In this study, at lower temperatures (30 °C and 50 °C), the parabolic model best fit the drying data for a conventional hot air oven, but at higher temperatures (70 °C), the page model showed the best fit.

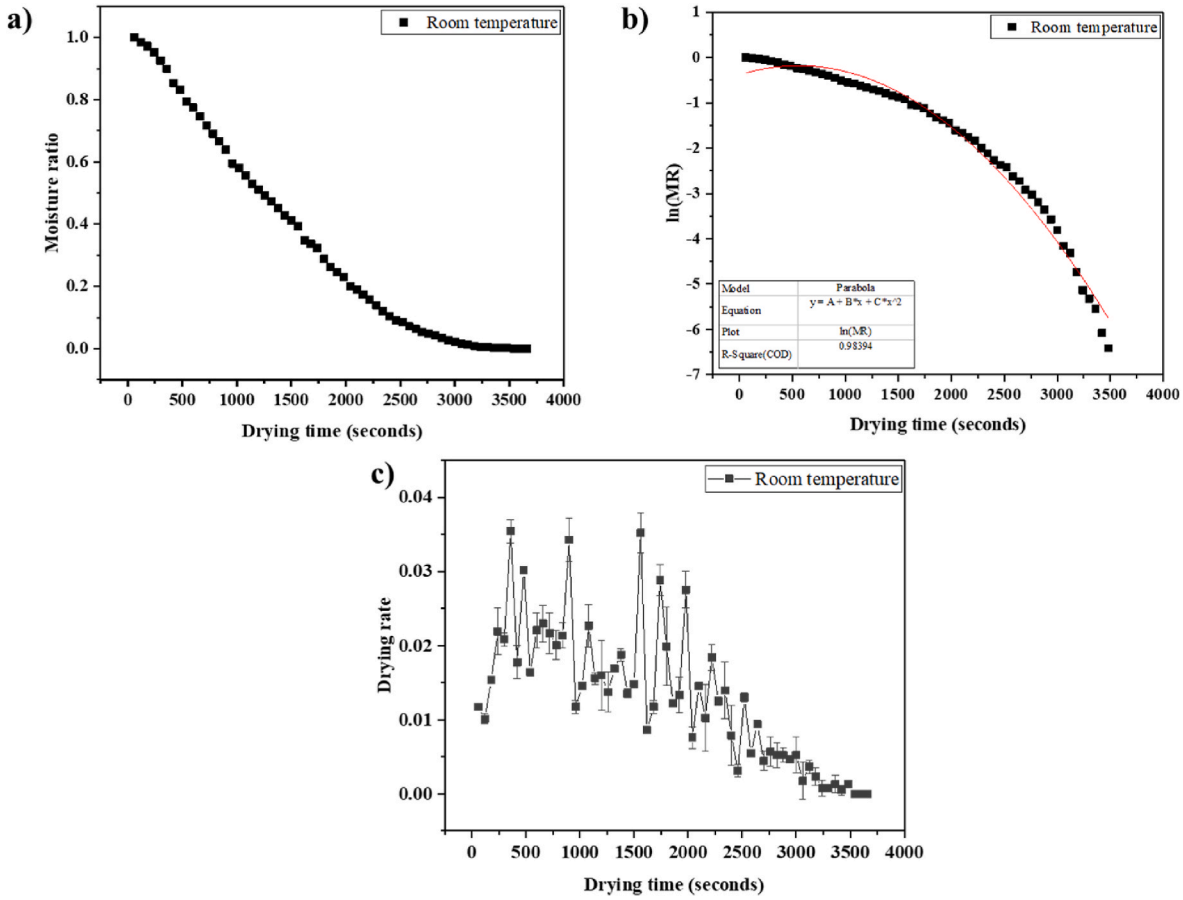

Fig. 3. a) Effect of drying time on the moisture content of *KBC*; b) Plot of ln *MR* vs. drying time; c) Drying rate curves of *KBC* at room temperature.

Table 3
Statistical analysis data for the modeling of moisture content and drying time for microwave oven-dried *KBC* films.

Drying conditions	Model	χ^2	R^2	Adjusted R^2	*SSE*	*RMSE*
P_180	Parabolic model	3.77E-4	0.9966	0.9964	0.0147	0.0194
	Wang and Singh	1.40E-3	0.9870	0.9867	0.0560	0.0374
	Vega-Lemus	3.75E-4	0.9965	0.9964	0.0150	0.0193
	Newton	0.67E-3	0.9363	0.9363	0.2758	0.0820
	Logarithmic	1.26E-3	0.9886	0.9880	0.0491	0.0355
	Two-term exponential	3.40E-3	0.9701	0.9678	0.1293	0.0583
	Modified Henderson and Pabis	6.88E-3	0.9381	0.9349	0.2681	0.0829
	Singh	1.33E-3	0.9886	0.9874	0.0491	0.0364
	Page	**1.77E-4**	**0.9983**	0.9983	0.0071	**0.0133**
	Midilli-Kucuk	1.29E-2	0.8869	0.87799	0.4902	0.1135
P_360	Parabolic model	6.56E-4	0.9943	0.9940	0.0249	0.0256
	Wang and Singh	1.72E-3	0.9848	0.9844	0.0671	0.0414
	Vega-Lemus	7.59E-4	0.9933	0.9931	0.0296	0.0275
	Newton	9.08E-3	0.9180	0.9180	0.3631	0.0952
	Logarithmic	1.20E-3	0.9897	0.9891	0.0456	0.0346
	Two-term exponential	5.33E-3	0.9555	0.9519	0.1970	0.0729
	Modified Henderson and Pabis	1.30E-3	0.9882	0.9897	0.0456	0.0361
	Singh	2.41E-3	0.9787	0.9782	0.0941	0.0491
	Page	**4.70E-4**	**0.9958**	0.9957	0.0183	**0.0217**
	Midilli-Kucuk	6.66E-3	0.9447	0.9402	0.2448	0.0813
P_540	Parabolic model	5.02E-4	0.9945	0.9944	0.0165	0.0224
	Wang and Singh	4.44E-4	0.9952	0.9950	0.0146	0.0210
	Vega-Lemus	4.45E-4	0.9952	0.9950	0.0146	0.0211
	Newton	3.29E-3	0.9635	0.9635	0.1117	0.0573
	Logarithmic	6.01E-4	0.9937	0.9933	0.0192	0.0245
	Two-term exponential	1.56E-3	0.9837	0.9827	0.0497	0.0394
	Modified Henderson and Pabis	1.72E-3	0.9837	0.9809	0.0497	0.0414
	Singh	1.54E-3	0.9833	0.9828	0.0508	0.0392
	Page	**3.93E-4**	**0.9958**	0.9956	0.0126	**0.0198**
	Midilli-Kucuk	1.50E-2	0.8471	0.8323	0.4678	0.1228
P_720	Parabolic model	1.03E-3	0.9915	0.9909	0.0278	0.0321
	Wang and Singh	3.19E-3	0.9728	0.9718	0.0894	0.0565
	Vega-Lemus	1.07E-3	0.9908	0.9905	0.0300	0.0327
	Newton	9.60E-3	0.9154	0.9154	0.2783	0.0979
	Logarithmic	2.33E-4	0.9809	0.9794	0.0629	0.0482
	Two-term exponential	5.08E-3	0.9568	0.9552	0.1422	0.0712
	Modified Henderson and Pabis	7.04E-3	0.9422	0.9379	0.1902	0.0839
	Singh	5.45E-3	0.9537	0.9520	0.1525	0.0738
	Page	**2.25E-4**	**0.9980**	0.9980	0.0063	**0.0150**
	Midilli-Kucuk	1.80E-2	0.8575	0.8410	0.4693	0.1343
P_900	Parabolic model	3.39E-4	0.9971	0.9968	0.0078	0.0184
	Wang and Singh	2.03E-3	0.9821	0.9814	0.0486	0.045
	Vega-Lemus	4.99E-4	0.9956	0.9954	0.0119	0.0223
	Newton	8.15E-3	0.9253	0.9253	0.2038	0.0902
	Logarithmic	0.14E-3	0.9876	0.9865	0.0338	0.0383
	Two-term exponential	3.58E-3	0.9711	0.9672	0.0787	0.0598
	Modified Henderson and Pabis	1.81E-2	0.8539	0.8340	0.3986	0.1346
	Singh	4.34E-3	0.9618	0.9602	0.1042	0.0659
	Page	**3.24E-4**	**0.9971**	0.9970	0.0077	**0.0180**
	Midilli-Kucuk	3.94E-3	0.9711	0.9639	0.0787	0.0627

(P: Microwave power levels).

3.2.3. Drying kinetics of KBC at room temperature

When the drying data of *KBC* samples at room temperature were fitted into different models, the R^2 ranged from 0.9307 to 0.9973, χ^2 ranged from 7.40E-3 to 2.99E-4, and *RMSE* ranged from 0.0862 to 0.0173 (Table 5). Similar to lower temperatures of conventional hot air oven drying, the parabolic model showed the lowest R^2 (0.9973), χ^2 (2.99E-4), and *RMSE* (0.0173) values. **Bhardwaj et al. (2017)** reported Midilli and Kucuk as the best model, whereas **Pinar et al. (2021)** reported Wang and Singh model as the best fit for predicting the shade drying behavior of *Vernonia amygdalina* leaves and red pepper, respectively. The difference in model selection may be largely due to the difference in the physical and chemical structure of the different dried materials. In the current study, the parabolic model best represented thin layer drying of KBC at room temperature.

3.3. Influence of drying methods on physical properties of KBC

BC films are rigid, lightweight, and moisture-free after drying; however, drying alters *BC*'s physical composition, affecting its properties and potential uses. Water molecules in the *BC* matrix or bound to the *BC* surface have two types of interactions-a) attached to the surface without chemical interaction and b) weak hydrogen bonding between *BC*'s hydroxyl (OH) groups and H_2O. Rapid evaporation of non-bonded water molecules does not disrupt the *BC* structure. Removing bound water molecules brings micro-fibrils closer, reinforcing and converting reversible hydrogen bonding interactions into irreversible ones. Dehydrated *BC*'s fluid absorption is greatly reduced by its reduced void spaces (**Ul-Islam *et al.*, 2013**). Thus, it is important to compare the water absorption, holding, and rehydration capacity of *BC* from the

Table 4
Statistical analysis data for the modeling of moisture content and drying time for the hot air oven-dried *KBC* films.

Drying conditions	Model	χ^2	R^2	Adjusted R^2	*SSE*	*RMSE*
HO_30 °C	Parabolic model	**5.12E-4**	**0.9952**	0.9949	0.0169	**0.0226**
	Wang and Singh	8.51E-4	0.9918	0.9916	0.0289	0.0291
	Vega-Lemus	7.23E-4	0.9931	0.9929	0.0246	0.0269
	Newton	7.39E-3	0.9275	0.9275	0.2586	0.0859
	Logarithmic	7.85E-4	0.9927	0.9923	0.0259	0.0280
	Two-term exponential	4.96E-3	0.9555	0.9513	0.15872	0.0704
	Modified Henderson and Pabis	5.29E-3	0.9555	0.9481	0.15872	0.0727
	Singh	1.24E-3	0.9882	0.9878	0.0420	0.0351
	Page	1.06E-3	0.9899	0.9896	0.0360	0.0325
	Midilli-Kucuk	4.05E-3	0.9637	0.9603	0.1295	0.0636
HO_50 °C	Parabolic model	**7.63E-4**	**0.9941**	0.9934	0.0145	**0.0276**
	Wang and Singh	1.9E-3	0.9843	0.9835	0.0387	0.0439
	Vega-Lemus	2.0E-3	0.9830	0.9821	0.0417	0.0457
	Newton	1.45E-2	0.8763	0.8763	0.3046	0.1204
	Logarithmic	8.50E-4	0.9934	0.9927	0.0161	0.0291
	Two-term exponential	8.88E-3	0.9351	0.9243	0.1598	0.0942
	Modified Henderson and Pabis	9.99E-3	0.9351	0.9148	0.1598	0.0999
	Singh	1.95E-3	0.9842	0.9834	0.0389	0.0441
	Page	1.11E-3	0.9909	0.9905	0.0222	0.0333
	Midilli-Kucuk	1.88E-3	0.9862	0.9839	0.0338	0.0433
HO_70 °C	Parabolic model	6.74E-4	0.9952	0.9945	0.087	0.0259
	Wang and Singh	4.60E-3	0.9644	0.9619	0.0654	0.0683
	Vega-Lemus	7.23E-4	0.9931	0.9929	0.0246	0.0269
	Newton	1.31E-2	0.8925	0.8925	0.1976	0.1147
	Logarithmic	1.59E-3	0.9887	0.9870	0.0206	0.0399
	Two-term exponential	5.22E-3	0.9659	0.9574	0.0626	0.0722
	Modified Henderson and Pabis	1.42E-2	0.8993	0.8838	0.1850	0.1193
	Singh	5.80E-3	0.9554	0.9523	0.0818	0.0764
	Page	**3.46E-4**	**0.9973**	0.9971	0.00485	**0.0186**
	Midilli-Kucuk	1.33E-2	0.9132	0.8915	0.1596	0.1153

(HO: Temperature of hot air oven).

Table 5
Statistical analysis data for the modeling of moisture content and drying time for the room temperature dried *KBC* films.

Drying conditions	Model	χ^2	R^2	Adjusted R^2	*SSE*	*RMSE*
RT	Parabolic model	**2.99E-4**	**0.9973**	0.9972	0.0173	**0.0173**
	Wang and Singh	1.10E-3	0.9895	0.9894	0.0671	0.0337
	Vega-Lemus	3.53E-4	0.9967	0.9967	0.0208	0.0188
	Newton	7.40E-3	0.9307	0.9307	0.4465	0.0862
	Logarithmic	7.51E-4	0.9932	0.9930	0.0435	0.0274
	Two-term exponential	4.00E-3	0.9639	0.9620	0.2326	0.0638
	Modified Henderson and Pabis	4.23E-3	0.9639	0.9606	0.2326	0.0650
	Singh	1.80E-3	0.9833	0.9830	0.1076	0.0427
	Page	5.24E-4	0.9952	0.9951	0.0309	0.0229
	Midilli-Kucuk	6.42E-3	0.9432	0.9402	0.3658	0.0801

(**RT: Room temperature**).

same source under different drying conditions to understand how physical and mechanical performance are interrelated.

3.3.1. Water absorption, holding capacity, and rehydration

From the plot of the water absorption capacity (*WAC*) of the *KBC* samples under different drying conditions (Fig. 4a), it can be seen that the maximum water absorption capacity was achieved at room temperature (56.54 ± 3.17 g/g). With a gradual increase in temperature in hot air oven drying and power levels in microwave oven drying, the water absorption capacity decreased. For the conventional hot air drying method, the maximum *WAC* was observed at 30 °C (55.43 ± 2.42 g/g), which was comparable with room temperature drying, and least at 70 °C (27.39 ± 0.68 g/g). In the microwave drying method, a steep decline can be seen in *WAC* values when the power was increased from 180 W (32.34 ± 3.71 g/g) to 900 W (16.91 ± 0.83 g/g). This can be attributed to the enhanced development of inter-fiber hydrogen bonding, which is favored at elevated temperatures and power levels during the processes of hot air oven drying and microwave drying, respectively. As a result, the capacity of the samples to undergo water absorption diminishes when temperature and power levels rise (**Andree *et al.*, 2021**). Thus, the application of different drying methods resulted in modifications to the pore structure and availability (**Sederavičiūtė *et al.*, 2019**), which led to a decrease in the water absorption capacity of dried *KBC*.

After freeze-drying the completely swelled *KBC* samples, they were weighed to compute the *WHC*, as shown in Fig. 4b. From the plot, it can be seen that similar to water absorption capacity, water holding capacity also decreased with an increase in temperature and power. Room temperature dried *KBC* showed a *WHC* of 87.06 ± 8.57 g/g, which was the highest amongst all the dried samples, and the closest value achieved was by oven drying at 30 °C (84.39 ± 6.87). Hot air oven-dried *KBC* samples showed a gradual decrease from 30 °C to 70 °C (48.16 ± 2.68 g/g). Microwave oven-dried samples showed a further decrease in *WHC* from 62.62 ± 1.59 g/g (at 180W) to 11.18 ± 1.57 g/g (at 900W). The reduction in water holding capacity (*WHC*) can be attributed to the

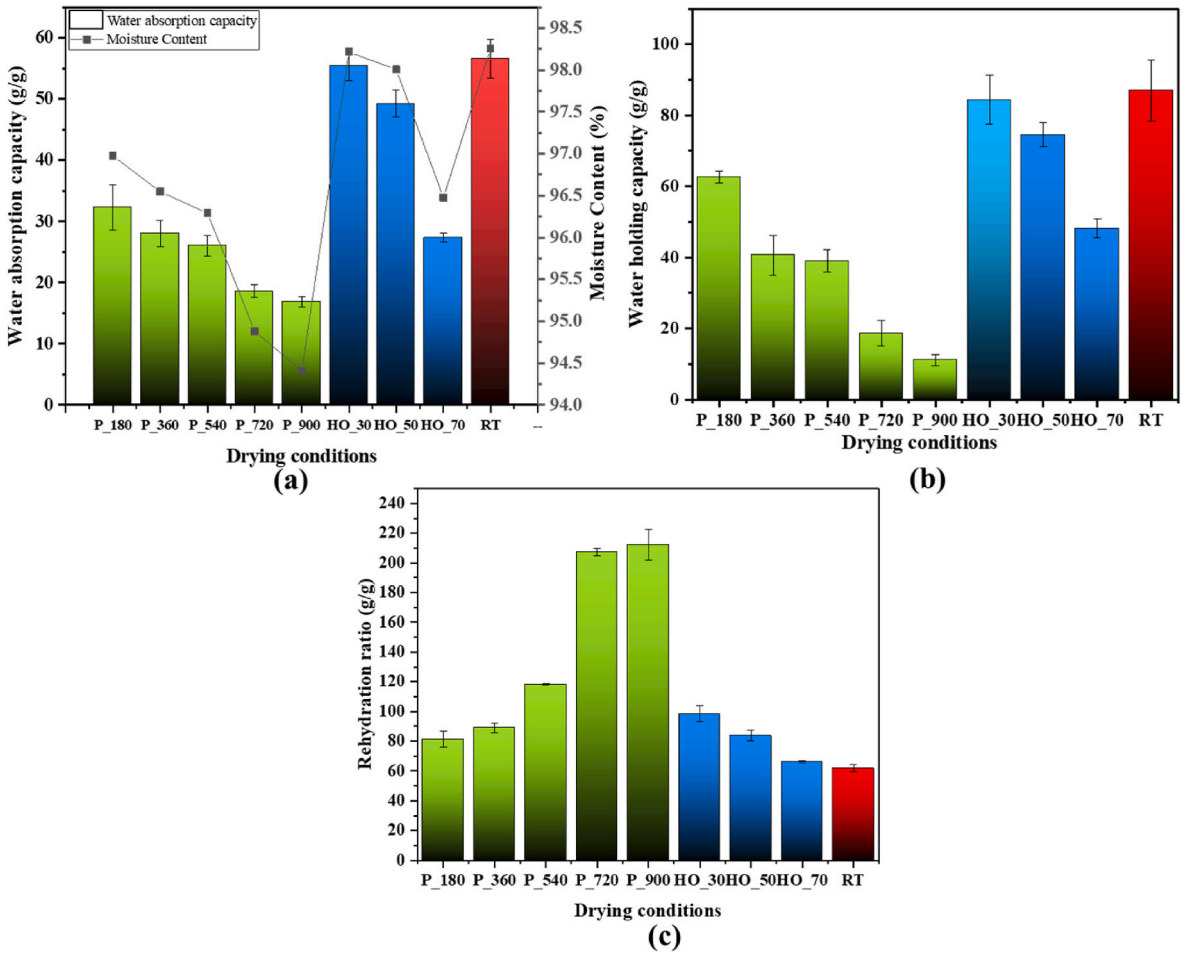

Fig. 4. Variation in (a) water absorption capacity and moisture content, (b) water holding capacity, (c) rehydration ratio of *KBC* after drying under different conditions (RT: Room temperature, HO: Temperature of hot air oven, P: Microwave power levels).

structural changes resulting from various drying processes, and higher levels of temperature and power may lead to cellulosic degradation. The process of drying leads to the extraction of water molecules, resulting in a reduction in the gaps between fibrils. Consequently, this also diminishes the ability of the fibrils to hold water molecules (**Ul-Islam *et al.*, 2013**). Similar trend was also reported during the drying of red pepper (**Deng *et al.*, 2018**; **Vega-Gálvez *et al.*, 2009**) and ginger slices (**Wang *et al.*, 2019**).

The rehydration ratios of *KBC* samples dried under different conditions have been represented in Fig. 4c, where it was observed that with increasing temperature, the rehydration ratio decreased, whereas contrastingly, with increasing power levels, the rehydration ratio increased. The contrasting results may be due to lower water holding capacity in microwave-dried samples, resulting in more free void spaces and, consequently, a higher rehydration ratio. It can also be coupled to the fact that the time taken in microwave drying was significantly lower than that of hot air oven drying, which led to minimum destruction in the structure of the *KBC* films. Similar trends for microwave drying were also reported by **Aydogdu et al. (2015)** and **Sorour and El-Mesery (2014)** for eggplants and onion slices, respectively. The rehydration capacity of dried products is notably influenced by various factors, including the drying conditions, pretreatments conducted before the drying process, and the textural characteristics of the final dried items. Similarly, the process of drying has the potential to reduce the osmotic characteristics of cell walls. Consequently, this leads to an increase in water absorption and volume, which is attributed to the swelling of hydrophilic substances such starch, cellulose, and pectin materials. The optimization of rehydration occurs when the extent of cellular structural disruption is minimized (**Vega-Gálvez et al., 2009**). In conventional hot air oven drying, the rehydration ratio decreased with an increase in temperature due to a comparatively higher drying period as compared to microwave drying, which led to structural damage, cell reduction, and altered pore structure (**Bodea et al., 2021**), ultimately reducing the rehydration capability. Similar observations were also reported by **Vega-Gálvez et al. (2009)** and **Aydogdu et al. (2015)**.

3.3.2. *Change in color intensity*

The investigation focused on analyzing the color of the dried *KBC* using *CIE* lightness (L^*), redness (a^*), and yellowness (b^*) values. A positive ΔL^* denotes lightning, and a negative ΔL^* indicates darkening (**Toker *et al.*, 2016**). The total difference in color, hue, and saturation was calculated using **Eqs. (21)–(23)** to characterize the variation during drying. From Table 6, it can be seen that with increasing temperature and power levels, the lightness (ΔL^*) decreased, but the total difference in saturation (ΔC^*) and hue (ΔH^*) of the samples increased. By increasing temperature in oven drying, an increase in the total difference in color (ΔE^*) between wet and dried *KBC* samples was observed, whereas, in the case of microwave drying, the total difference in color decreased, possibly due to lesser drying durations leading to preservation of surface color. An increase in yellowness (b^*) of the samples may be due to the formation of brown components resulting from non-enzymatic reactions (**Vega-Gálvez *et al.*, 2009**), with oven-dried samples showing higher yellowness. The *KBC* films also showed an increase in redness (a^*) of the samples with the highest values for microwave drying, compared to hot air oven and room temperature drying. The occurrence of Maillard reactions during the process of microwave

Table 6
Variation in chromatic coordinates of dried *KBC* samples after drying.

Sample	*ΔL**	*A**	*B**	*ΔE**	*ΔC**	*ΔH**
MICROWAVE DRYING						
P_180	**−22.07**	−0.25	6.96	24.11	3.73	10.41
P_360	−21.46	−0.41	7.64	23.85	4.41	11.29
P_540	−18.07	0.04	9.61	21.91	6.37	13.94
P_720	−16.44	0.15	10.98	21.44	7.74	15.80
P_900	−10.80	**0.92**	**13.04**	**19.25**	**9.84**	**18.72**
HOT AIR OVEN DRYING						
HO_30	**−21.04**	−1.00	9.64	**24.38**	6.45	13.91
HO_50	−19.98	−0.83	13.28	25.57	10.07	18.87
HO_70	−16.75	**0.88**	**19.68**	28.04	**16.46**	**27.88**
ROOM TEMPERATURE DRYING						
RT	−21.31	−0.59	9.11	24.37	5.89	13.21

(RT: Room temperature, HO: Temperature of hot air oven, P: Microwave power levels).

drying may cause this phenomenon. Room temperature or shade drying showed values similar to oven drying at 30 °C. Similar results were also reported for eggplant drying by a combination of microwave-IR drying and hot air oven drying (**Aydogdu *et al.*, 2015**).

3.3.3. Other physical properties

The reinforcement of hydrogen bonding from water evaporation improves *BC*'s mechanical characteristics and industrial uses. Few studies have reported *BC* films as brittle, possessing high tensile strength and elastic modulus values, but exhibiting low strain at breakage, which depends upon the specific fermentation circumstances (static or agitated culture, air supplementation, reactor design), as well as the film processing techniques employed **(Ramírez Tapias *et al.*, 2022)**. The tensile strength can be seen (Fig. S1) to increase linearly for hot air oven samples with a maximum tensile strength of 57.09 ± 0.75 MPa at 70 °C. The tensile strength at room temperature (44.87 ± 2.10 MPa) was similar to that of the oven-dried sample (44.27 ± 4.51 MPa) at 30 °C; for microwave samples, the tensile strength can be seen to decrease from power level at 180 W (59.45 ± 6.44 MPa) to the least at 900 W (4.99 ± 2.55 MPa). The strain of material pertains to the extent of potential deformation that a material may undergo when subjected to an externally applied force **(Ul-Islam *et al.*, 2013)**. The strain can be seen (Table S1) to reduce as the temperature and power level were increased. Young's modulus is a physical property that may be observed as the initial slope of the curves, which serves as a quantitative measure of the stiffness of a material **(Clasen *et al.*, 2006)**. It was observed that with increasing power levels and temperature, the stiffness of the material also increased, indicating that it loses its elasticity and becomes more brittle. Lower power levels help to preserve the porous structure, strength, and deformation properties of the material. It was further observed that except for the films dried at *RT* and 30 °C, for all the other samples, the critical value of Young's modulus of 755 MPa, as discussed by **Clasen et al. (2006)** was exceeded. Membranes possessing Young's moduli over this key threshold exhibit inadequate elasticity to withstand the requisite levels of bending or stretching during commercial application.

The BC material is comprised of a composite structure consisting of cellulose, specifically I_α and I_β, which coexist. The I_α polymorph is the dominant form of cellulose derived from bacteria. However, following alkaline treatment or hydrothermal annealing, the I_α polymorph undergoes a partial transformation to the I_β polymorph. Additionally, it is possible to transform cellulose into the more stable crystalline structure known as cellulose II **(Zeng et al., 2014)**. The *XRD* analysis of dried *KBC* films revealed with varying temperature and power levels, the intensity of the peaks differed with two distinct peaks at 2θ values of ~14.3° and ~22.6°, which can be attributed to the crystalline planes (100) and (110), respectively. Additionally, a minor peak was observed at 16.6°, originating from the (010) plane. The amorphous area is indicative of the non-crystalline component of the BC material and is used in the estimation of its relative crystallinity. The proportion between the crystalline and amorphous regions exhibits variability across different samples and is dependent upon a range of factors, encompassing the source of the biopolymer composite (*BC*), the microorganism involved, the content of the medium, and the circumstances employed during processing. The crystallinity values of *KBC* samples was observed to be maximum at 50 °C (78.44%) for oven dried samples and at 540 W (73.32%) for microwave dried samples (Table S2). The crystallinity gradually increased followed by a decrease when the temperature and power levels were further increased. But in this study, as the *KBC* samples were obtained from the same source without any variation in media components or microorganisms involved or post-harvest NaOH treatment, it is safe to assume that the variations occurred solely due to difference in drying conditions. The d-spacing values were similar for oven drying, room temperature drying and microwave drying at 180 W. For higher power levels, the d-spacing values showed a slight difference which may be attributed to variation in cross-sectional dimension of cellulose crystallites due to drying at increased power levels **(Castro et al., 2011)**. A similar observation of increased crystallinity values was also reported by **Ul-Islam et al. (2013)**, who explained this phenomenon of annealing when polymers are subjected to specific temperatures below their crystalline phase. This process provides the necessary energy and time for the molecular chains to rectify the defects in crystal packing and align themselves within an ideal crystal lattice structure.

The sessile drop method or contact angle analysis was used to determine the change in wettability of *KBC* films due to drying conditions Fig.S2. It was observed that the hydrophilicity slightly decreased for oven-dried samples but drastically decreased for microwave samples, corroborating the water absorption data.

4. Conclusion

In conclusion, this work demonstrated the effect of different drying conditions on the intrinsic properties of *KBC* films. With an increase in temperature and power, the moisture removal and drying rate increased, but the drying time decreased. A lower activation energy of 131.70 Wg^{-1}, higher moisture diffusivity of 48.27*10^{-11} m^2s^{-1}, and greater tensile strength of 59.45 MPa were exhibited by the microwave drying method. The highest crystallinity of 78.44% was demonstrated by hot air oven-dried KBC samples at 50 °C. Out of the ten kinetic models, Page and parabolic models best described the drying data under different drying conditions. It can be concluded that microwave drying proved to be a more efficient method based on less time, lesser activation energy, higher rehydration ratio, and tensile strength, whereas room temperature drying proved to be a better method based on affinity towards water.

CRediT authorship contribution statement

Baishali Dey: Writing – original draft, Visualization, Validation, Methodology, Investigation, Formal analysis, Data curation, Conceptualization. **Sivaraman Jayaraman:** Supervision. **Paramasivan Balasubramanian:** Writing – review & editing, Supervision, Resources, Project administration, Funding acquisition, Conceptualization.

Declaration of competing interest

The authors declare that they have no known competing financial interests or personal relationships that could have appeared to influence the work reported in this paper.

Data availability

Data will be made available on request.

Acknowledgments

The authors are grateful to the Department of Biotechnology and Medical Engineering, NIT Rourkela, for providing their research facilities. The authors greatly acknowledge the Ministry of Education, Government of India for sponsoring the PhD program of the first author.

This research did not receive any specific grant from funding agencies in the public, commercial, or not-for-profit sectors.

Appendix ASupplementary data

Supplementary data to this article can be found online at https://doi.org/10.1016/j.jclepro.2024.142204.

References

Aduri, P., Ankita Rao, K., Fatima, A., Kaul, P., Shalini, A., 2019. STUDY OF BIODEGRADABLE PACKAGING MATERIAL PRODUCED FROM SCOBY. https://doi.org/10.26479/2019.0503.32.

Agbede, O.O., Oke, E.O., Akinfenwa, S.I., Wahab, K.T., Ogundipe, S., Aworanti, O.A., Arinkoola, A.O., Agarry, S.E., Ogunleye, O.O., Osuolale, F.N., Babatunde, K.A., 2020. Thin layer drying of green microalgae (Chlorella sp.) paste biomass: drying characteristics, energy requirement and mathematical modeling. Bioresour. Technol. Rep. 11, 100467 https://doi.org/10.1016/j.biteb.2020.100467.

Alara, O.R., Abdurahman, N.H., Abdul Mudalip, S.K., Olalere, O.A., 2018. Mathematical modeling of thin layer drying using open sun and shade of Vernonia amygdalina leaves. Agric. Nat. Resour. 52, 53–58. https://doi.org/10.1016/J.ANRES.2018.05.013.

Amarasekara, A.S., Wang, D., Grady, T.L., 2020. A comparison of kombucha SCOBY bacterial cellulose purification methods. SN Appl. Sci. 2, 1–7. https://doi.org/10.1007/S42452-020-1982-2/FIGURES/4.

Andree, V., Niopek, D., Müller, C., Eiselt, J.P., Foh, N., Rzany, A., Hensel, B., 2021. Influence of drying methods on the physical properties of bacterial nanocellulose. Mater. Res. Express 8, 025402. https://doi.org/10.1088/2053-1591/ABE016.

Antolak, H., Piechota, D., Kucharska, A., 2021. Kombucha tea—a double power of bioactive compounds from tea and symbiotic culture of bacteria and yeasts (SCOBY). Antioxidants 10 (2021), 1541. https://doi.org/10.3390/ANTIOX10101541. Page 1541 10.

Aydogdu, A., Sumnu, G., Sahin, S., 2015. Effects of microwave-infrared combination drying on quality of eggplants. Food Bioprocess Technol. 8, 1198–1210. https://doi.org/10.1007/S11947-015-1484-1/FIGURES/10.

Behera, B., Balasubramanian, P., 2021. Experimental and modelling studies of convective and microwave drying kinetics for microalgae. Bioresour. Technol. 340, 125721 https://doi.org/10.1016/J.BIORTECH.2021.125721.

Bhardwaj, A.K., Chauhan, R., Kumar, R., Sethi, M., Rana, A., 2017. Experimental investigation of an indirect solar dryer integrated with phase change material for drying valeriana jatamansi (medicinal herb). Case Stud. Therm. Eng. 10, 302–314. https://doi.org/10.1016/J.CSITE.2017.07.009.

Bhardwaj, A.K., Kumar, R., Chauhan, R., 2019. Experimental investigation of the performance of a novel solar dryer for drying medicinal plants in Western Himalayan region. Sol. Energy 177, 395–407. https://doi.org/10.1016/J.SOLENER.2018.11.007.

Biswas, R., Hossain, M.A., Zzaman, W., 2022. Thin layer modeling of drying kinetics, rehydration kinetics and color changes of osmotic pre-treated pineapple (Ananas comosus) slices during drying: development of a mechanistic model for mass transfer. Innovat. Food Sci. Emerg. Technol. 80, 103094 https://doi.org/10.1016/J.IFSET.2022.103094.

Bodea, I.M., Beteg, F.I., Pop, C.R., David, A.P., Dudescu, M.C., Vilău, C., Stănilă, A., Rotar, A.M., Cătunescu, G.M., 2021. Optimization of moist and oven-dried bacterial cellulose production for functional properties. Polymers 13, 2088. https://doi.org/10.3390/POLYM13132088/S1.

Bueno, F., Spivak, D.A., Sathivel, S., 2023. Evaluation of the properties of dry bacterial cellulose synthesized from coffee kombucha fermentation dried with different drying methods. Dry. Technol. https://doi.org/10.1080/07373937.2023.2274402.

Castro, C., Zuluaga, R., Putaux, J.L., Caro, G., Mondragon, I., Gañán, P., 2011. Structural characterization of bacterial cellulose produced by Gluconacetobacter swingsii sp. from Colombian agroindustrial wastes. Carbohydr. Polym. 84, 96–102. https://doi.org/10.1016/J.CARBPOL.2010.10.072.

Chang, W.S., Chen, H.H., 2016. Physical properties of bacterial cellulose composites for wound dressings. Food Hydrocolloids 53, 75–83. https://doi.org/10.1016/J.FOODHYD.2014.12.009.

Chayjan, R.A., Parian, J.A., Esna-Ashari, M., 2011. Modeling of moisture diffusivity, activation energy and specific energy consumption of high moisture corn in a fixed and fluidized bed convective dryer. Spanish J. Agric. Res. 9, 28–40. https://doi.org/10.5424/SJAR/20110901-077-10.

Clasen, C., Sultanova, B., Wilhelms, T., Heisig, P., Kulicke, W.M., 2006. Effects of different drying processes on the material properties of bacterial cellulose membranes. Macromol. Symp. 244, 48–58. https://doi.org/10.1002/MASY.200651204.

Darvishi, H., Azadbakht, M., Rezaeiasl, A., Farhang, A., 2013. Drying characteristics of sardine fish dried with microwave heating. J. Saudi Soc. Agric. Sci. 12, 121–127. https://doi.org/10.1016/J.JSSAS.2012.09.002.

Demiray, E., Seker, A., Tulek, Y., 2017. Drying kinetics of onion (Allium cepa L.) slices with convective and microwave drying. Heat Mass Transf. und Stoffuebertragung 53, 1817–1827. https://doi.org/10.1007/S00231-016-1943-X/FIGURES/9.

Deng, L.Z., Yang, X.H., Mujumdar, A.S., Zhao, J.H., Wang, D., Zhang, Q., Wang, J., Gao, Z.J., Xiao, H.W., 2018. Red pepper (Capsicum annuum L.) drying: effects of different drying methods on drying kinetics, physicochemical properties, antioxidant capacity, and microstructure. Dry. Technol. 36, 893–907. https://doi.org/10.1080/07373937.2017.1361439.

Doymaz, I., 2006. Drying kinetics of black grapes treated with different solutions. J. Food Eng. 76, 212–217. https://doi.org/10.1016/J.JFOODENG.2005.05.009.

Doymaz, I., Smail, O., 2011. Drying characteristics of sweet cherry. Food Bioprod. Process. 89, 31–38. https://doi.org/10.1016/J.FBP.2010.03.006.

El-Wakil, N.A., Hassan, E.A., Hassan, M.L., Abd El-Salam, S.S., 2019. Bacterial cellulose/phytochemical's extracts biocomposites for potential active wound dressings. Environ. Sci. Pollut. Res. 26, 26529–26541. https://doi.org/10.1007/S11356-019-05776-W/FIGURES/4.

Gregory, D.A., Tripathi, L., Fricker, A.T.R., Asare, E., Orlando, I., Raghavendran, V., Roy, I., 2021. Bacterial cellulose: a smart biomaterial with diverse applications. Mater. Sci. Eng. R Rep. 145, 100623 https://doi.org/10.1016/J.MSER.2021.100623.

Guiné, R.P.F., 2010. Analysis of the drying kinetics of S. Bartolomeu pears for different drying systems. Electron. J. Environ. Agric. Food Chem. 9, 1772–1783.

Harrison, K., Curtin, C., 2021. Microbial composition of scoby starter cultures used by commercial kombucha brewers in North America. Microorganisms 9, 1060. https://doi.org/10.3390/MICROORGANISMS9051060/S1.

İlter, I., Akyıl, S., Devseren, E., Okut, D., Koç, M., Kaymak Ertekin, F., 2018. Microwave and hot air drying of garlic puree: drying kinetics and quality characteristics. Heat Mass Transf. und Stoffuebertragung 54, 2101–2112. https://doi.org/10.1007/S00231-018-2294-6/FIGURES/3.

Inyang, U.E., Oboh, O., Etuk, B.R., 2018. Kinetic models for drying techniques-food materials. Adv. Chem. Eng. Sci. 8, 27–48. https://doi.org/10.4236/aces.2018.82003.

Kalaiappan, K., Rengapillai, S., Marimuthu, S., Murugan, R., Thiru, P., 2020. Kombucha SCOBY-based carbon and graphene oxide wrapped sulfur/polyacrylonitrile as a high-capacity cathode in lithium-sulfur batteries. Front. Chem. Sci. Eng. 14, 976–987. https://doi.org/10.1007/S11705-019-1897-X/METRICS.

Kamiński, K., Jarosz, M., Grudzień, J., Pawlik, J., Zastawnik, F., Pandyra, P., Kołodziejczyk, A.M., 2020. Hydrogel bacterial cellulose: a path to improved materials for new eco-friendly textiles. Cellulose 27, 5353–5365. https://doi.org/10.1007/S10570-020-03128-3/FIGURES/7.

Kaya, A., Aydin, O., Demirtaş, C., 2007. Drying kinetics of red delicious apple. Biosyst. Eng. 96, 517–524. https://doi.org/10.1016/J.BIOSYSTEMSENG.2006.12.009.

Laavanya, D., Shirkole, S., Balasubramanian, P., 2021. Current challenges, applications and future perspectives of SCOBY cellulose of Kombucha fermentation. J. Clean. Prod. https://doi.org/10.1016/j.jclepro.2021.126454.

Lin, W.C., Lien, C.C., Yeh, H.J., Yu, C.M., Hsu, S.H., 2013. Bacterial cellulose and bacterial cellulose–chitosan membranes for wound dressing applications. Carbohydr. Polym. 94, 603–611. https://doi.org/10.1016/J.CARBPOL.2013.01.076.

Midilli, A., Kucuk, H., Yapar, Z., 2002. A new model for single-layer drying. Dry. Technol. 20, 1503–1513. https://doi.org/10.1081/DRT-120005864.

Mohamad, S., Abdullah, L.C., Jamari, S.S., Al Edrus, S.S.O., Aung, M.M., Mohamad, S.F.S., 2022. Influence of drying method on the crystal structure and thermal property of oil palm frond juice-based bacterial cellulose. J. Mater. Sci. 57, 1462–1473. https://doi.org/10.1007/S10853-021-06685-5/FIGURES/6.

Mohapatra, D., Rao, P.S., 2005. A thin layer drying model of parboiled wheat. J. Food Eng. 66, 513–518. https://doi.org/10.1016/J.JFOODENG.2004.04.023.

Mousavi, S.M., Hashemi, S.A., Zarei, M., Gholami, A., Lai, C.W., Chiang, W.H., Omidifar, N., Bahrani, S., Mazraedoost, S., 2020. Recent progress in chemical composition, production, and pharmaceutical effects of kombucha beverage: a complementary and alternative medicine. Evid. base Compl. Alternative Med. 2020 https://doi.org/10.1155/2020/4397543.

Nguyen, H.T., Saha, N., Ngwabebhoh, F.A., Zandraa, O., Saha, T., Saha, P., 2021. Kombucha-derived bacterial cellulose from diverse wastes: a prudent leather alternative. Cellulose 28, 9335–9353. https://doi.org/10.1007/S10570-021-04100-5/FIGURES/9.

Nguyen, T.V.L., Nguyen, M.D., Nguyen, D.C., Bach, L.G., Lam, T.D., 2019. Model for thin layer drying of lemongrass (cymbopogon citratus) by hot air. Processes 7 (2019), 21. https://doi.org/10.3390/PR7010021. Page 21 7.

Olanipekun, B.F., Tunde-Akintunde, T.Y., Oyelade, O.J., Adebisi, M.G., Adenaya, T.A., 2015. Mathematical modeling of thin-layer pineapple drying. J. Food Process. Preserv. 39, 1431–1441. https://doi.org/10.1111/jfpp.12362.

Perea-Flores, M.J., Garibay-Febles, V., Chanona-Pérez, J.J., Calderón-Domínguez, G., Méndez-Méndez, J.V., Palacios-González, E., Gutiérrez-López, G.F., 2012. Mathematical modelling of castor oil seeds (Ricinus communis) drying kinetics in fluidized bed at high temperatures. Ind. Crops Prod. 38, 64–71. https://doi.org/10.1016/J.INDCROP.2012.01.008.

Pillai, M.M., Tran, H.N., Sathishkumar, G., Manimekalai, K., Yoon, J.H., Lim, D.Y., Noh, I., Bhattacharyya, A., 2021. Symbiotic culture of nanocellulose pellicle: a potential matrix for 3D bioprinting. Mater. Sci. Eng. C 119, 111552. https://doi.org/10.1016/J.MSEC.2020.111552.

Pinar, H., Çetin, N., Ciftci, B., Karaman, K., Kaplan, M., 2021. Biochemical composition, drying kinetics and chromatic parameters of red pepper as affected by cultivars and drying methods. J. Food Compos. Anal. 102, 103976 https://doi.org/10.1016/J.JFCA.2021.103976.

Ramírez Tapias, Y.A., Di Monte, M.V., Peltzer, M.A., Salvay, A.G., 2022. Bacterial cellulose films production by Kombucha symbiotic community cultured on different herbal infusions. Food Chem. 372, 131346 https://doi.org/10.1016/J.FOODCHEM.2021.131346.

Ruan, C., Zhu, Y., Zhou, X., Abidi, N., Hu, Y., Catchmark, J.M., 2016. Effect of cellulose crystallinity on bacterial cellulose assembly. Cellulose 23, 3417–3427. https://doi.org/10.1007/S10570-016-1065-0/FIGURES/7.

Sederavičiūtė, F., Domskienė, J., Baltina, I., 2019. Influence of drying temperature on tensile and bursting strength of bacterial cellulose biofilm. Mater. Sci. 25, 316–321. https://doi.org/10.5755/J01.MS.25.3.20764.

Sharma, G.P., Prasad, S., 2004. Effective moisture diffusivity of garlic cloves undergoing microwave-convective drying. J. Food Eng. 65, 609–617. https://doi.org/10.1016/J.JFOODENG.2004.02.027.

Singh, G.D., Sharma, R., Bawa, A.S., Saxena, D.C., 2008. Drying and rehydration characteristics of water chestnut (Trapa natans) as a function of drying air temperature. J. Food Eng. 87, 213–221. https://doi.org/10.1016/j.jfoodeng.2007.11.027.

Soares, M.G., de Lima, M., Reolon Schmidt, V.C., 2021. Technological aspects of kombucha, its applications and the symbiotic culture (SCOBY), and extraction of compounds of interest: a literature review. Trends Food Sci. Technol. 110, 539–550. https://doi.org/10.1016/J.TIFS.2021.02.017.

Song, Z., Yao, L., Jing, C., Zhao, X., Wang, W., Sun, J., Mao, Y., Ma, C., 2016. Elucidation of the pumping effect during microwave drying of lignite. ACS Publ 55, 3167–3176. https://doi.org/10.1021/acs.iecr.5b04881.

Sorour, H., El-Mesery, H., 2014. Impact factor(JCC): 1.4507-EFFECT of microwave and infrared radiation on drying OF ONION slices. impactjournals.usH Sorour, H El-MeseryInt.. J. Res. Appl. Nat. Soc. Sci, 2014•impactjournals.us 2, 119–130.

Stumpf, T.R., Pértile, R.A.N., Rambo, C.R., Porto, L.M., 2013. Enriched glucose and dextrin mannitol-based media modulates fibroblast behavior on bacterial cellulose membranes. Mater. Sci. Eng. C 33, 4739–4745. https://doi.org/10.1016/J.MSEC.2013.07.035.

Toğrul, I.T., Pehlivan, D., 2004. Modelling of thin layer drying kinetics of some fruits under open-air sun drying process. J. Food Eng. 65, 413–425. https://doi.org/10.1016/J.JFOODENG.2004.02.001.

Toker, H., Baysal, E., Türkoğlu, T., Kart, Ş., Şen, F., Peker, H., 2016. Surface Characteristics of Oriental Beech and Scots Pine Woods Heat-Treated above 200 Degrees C.

Ul-Islam, M., Khattak, W.A., Kang, M., Kim, S.M., Khan, T., Park, J.K., 2013. Effect of post-synthetic processing conditions on structural variations and applications of bacterial cellulose. Cellulose 20, 253–263. https://doi.org/10.1007/S10570-012-9799-9/FIGURES/6.

Vega-Gálvez, A., Di Scala, K., Rodríguez, K., Lemus-Mondaca, R., Miranda, M., López, J., Perez-Won, M., 2009. Effect of air-drying temperature on physico-chemical properties, antioxidant capacity, colour and total phenolic content of red pepper (Capsicum annuum, L. var. Hungarian). Food Chem. 117, 647–653. https://doi.org/10.1016/J.FOODCHEM.2009.04.066.

Vega-Gálvez, A., Miranda, M., Díaz, L.P., Lopez, L., Rodriguez, K., Scala, K. Di, 2010. Effective moisture diffusivity determination and mathematical modelling of the drying curves of the olive-waste cake. Bioresour. Technol. 101, 7265–7270. https://doi.org/10.1016/J.BIORTECH.2010.04.040.

Wang, D., Dai, J.W., Ju, H.Y., Xie, L., Xiao, H.W., Liu, Y.H., Gao, Z.J., 2015. Drying kinetics of American ginseng slices in thin-layer air impingement dryer. Int. J. Food Eng. 11, 701–711. https://doi.org/10.1515/IJFE-2015-0002/MACHINEREADABLECITATION/RIS.

Wang, J., Bai, T.Y., Wang, D., Fang, X.M., Xue, L.Y., Zheng, Z.A., Gao, Z.J., Xiao, H.W., 2019. Pulsed vacuum drying of Chinese ginger (Zingiber officinale Roscoe) slices: effects on drying characteristics, rehydration ratio, water holding capacity, and microstructure. Dry. Technol. 37, 301–311. https://doi.org/10.1080/07373937.2017.1423325.

Wang, Z., Sun, J., Liao, X., Chen, F., Zhao, G., Wu, J., Hu, X., 2007. Mathematical modeling on hot air drying of thin layer apple pomace. Food Res. Int. 40, 39–46. https://doi.org/10.1016/J.FOODRES.2006.07.017.

Zarein, M., Samadi, S.H., Ghobadian, B., 2015. Investigation of microwave dryer effect on energy efficiency during drying of apple slices. J. Saudi Soc. Agric. Sci. 14, 41–47. https://doi.org/10.1016/J.JSSAS.2013.06.002.

Zeng, M., Laromaine, A., Roig, A., 2014. Bacterial cellulose films: influence of bacterial strain and drying route on film properties. Cellulose 21, 4455–4469. https://doi.org/10.1007/S10570-014-0408-Y/TABLES/3.